Desalination and Water Treatment
www.deswater.com

doi: 10.1080/19443994.2015.1125797

57 (2016) 22017–22028
October

Taylor & Francis
Taylor & Francis Group

Photocatalytic degradation of reactive red 3 and alachlor over uncalcined Fe–TiO_2 synthesized via hydrothermal method

K.K.P. Rivera[a,b], M.D.G. de Luna[c], T. Suwannaruang[b,d], K. Wantala[b,d,e,*]

[a]*Environmental Engineering Program, National Graduate School of Engineering, University of the Philippines, 1101 Diliman, Quezon City, Philippines, Tel. +632 981 8500, local 3114; email: kprivera@up.edu.ph*
[b]*Chemical Kinetics and Applied Catalysis Laboratory (CKCL), Faculty of Engineering, Khon Kaen University, Khon Kaen 40002, Thailand, Tel. +664 336 2240; email: totsaporn.eng.kku@gmail.com (T. Suwannaruang), Tel. +664 336 2240, ext. 45705; Fax: +664 336 2240; email: kitirote@kku.ac.th (K. Wantala)*
[c]*Department of Chemical Engineering, University of the Philippines, 1101 Diliman, Quezon City, Philippines, Tel. +632 981 8500, local 3114; Fax: +632 929 6640; emails: mgdeluna@up.edu.ph, mgdeluna@gmail.com*
[d]*Faculty of Engineering, Department of Chemical Engineering, Khon Kaen University, Khon Kaen 40002, Thailand*
[e]*Research Center for Environmental and Hazardous Substance Management (EHSM), Faculty of Engineering, Khon Kaen University, Khon Kaen 40002, Thailand*

Received 6 March 2015; Accepted 22 November 2015

ABSTRACT

In this work, Fe^{3+} was used to modify TiO_2 to give improved performance under UV and visible light irradiation. The catalysts were prepared via a hydrothermal method without further calcination. Box–Behnken design was used to investigate the effects of hydrothermal temperature, hydrothermal time, and Fe content (wt%) on the photocatalytic performance of TiO_2. Pollutants such as reactive red 3 (RR3) dye and alachlor were examined. The synthesized catalysts have been characterized by many techniques. Photodegradation of RR3 dye was performed under UV light irradiation whereas photodegradation of alachlor was performed under both UV and visible light irradiation. In RR3 photodegradation, the effect hydrothermal settings for temperature and time were found significant and the highest removal percentages were 92 and 94% for 15 and 30 min UV irradiation, respectively. In alachlor photodegradation, the effect of Fe-doping was found significant under both UV and visible light irradiation. The highest removal percentages were 49 and 82% for 15 and 30 min of UV light irradiation, respectively, and 51% for 60 min of visible light irradiation. Only anatase crystallite was found in catalysts with and without Fe. Energy band gaps decreased with increasing Fe contents. The crystallite sizes of catalysts with 0.10 wt% Fe^{3+} content decreased with increasing hydrothermal time and temperature, while surface area increased. Energy-dispersive X-ray spectroscopy technique was able to detect nitrogen contents of about 10 wt% and X-ray absorption near edge structure was used to find the oxidation states of Fe^{3+} and $Fe^{3+/4+}$ in Fe–TiO_2 as well.

Keywords: Alachlor; Box–Behnken design; Fe–TiO_2; Photocatalysis; Dye

*Corresponding author.

1. Introduction

Titanium dioxide is a promising photocatalyst in wastewater treatment. Its excellent properties include photostability, self-cleaning ability, non-toxicity, and low cost [1,2]. It is commonly used in the industry as a commercial photocatalyst and has also been the subject of many researches that focus on the removal of organics in water [1,3]. However, there are a number of limitations to the use of this material in a wider scale than a laboratory setup [1].

The ability to generate electron–hole pairs that facilitate the photocatalytic process can be hindered by high recombination rates [4–6]. Recombination inhibits the movement of the photogenerated electron–hole pairs, rendering them useless and unable to participate in the photocatalytic reactions [7,8]. Light with energy higher than the energy band gap of TiO_2, i.e. UV light ($\lambda = 365$ nm), should be utilized in order to mobilize the photogenerated electron–hole pairs [2,6,8–13]. Thus, this limits the activity of TiO_2 to photocatalysis under UV light irradiation, which only makes up a very small portion of solar light [2,8,14].

Metal doping on TiO_2 has been introduced to address the limitation of its use under UV light irradiation only [2,4,8,15–18]. The addition of Fe^{3+} improves the photocatalytic activity of TiO_2 [17,19–21]. First, it acts as electron traps by capturing the photogenerated electrons and prevents the recombination with the photogenerated holes and thus, decreases the recombination rate [19,22]. It also reduces the energy band gap, resulting in increased activity under light with longer wavelengths, i.e. visible light ($\lambda > 400$ nm) [5,19,22–24].

Fe–TiO_2 could remove an array of environmental pollutants from wastewater ranging from dyes to recalcitrant compounds [19,25]. The dark colors of dyes in wastewater have adverse effects since it is toxic to aquatic life, prevents sunlight penetration to the water, and is visible even in low concentrations [26,27]. On the other hand, colorless organic compounds, such as alachlor, also pose a similar threat. The wide usage of alachlor as an herbicide for agricultural crops makes it very easy for it to contaminate water resources [28,29]. It is also considered to be a high health hazard since it has been listed as a carcinogenic compound [28].

It is important to find a photocatalyst that is suitable in systems that do not only involve different light sources, i.e. UV and visible light irradiation, but also pollutants with different physical properties such as RR3 dye, which has a dark color, and alachlor, which is colorless. The application of modified TiO_2 photocatalysts to such systems extends the understanding of its light-gathering capabilities and the effects of Fe^{3+} in its improvement.

Hydrothermal techniques for Fe–TiO_2 synthesis usually report a single-step heat treatment, a subsequent drying step, and finally, a calcination step at temperatures of at least 300˚C. Shorter hydrothermal time usually requires a higher hydrothermal temperature [20]. Consequently, for a lower hydrothermal temperature, a longer hydrothermal time would also be necessary [22]. Both studies were able to produce photocatalysts that are composed of anatase TiO_2. Finding a suitable hydrothermal treatment that will promote anatase TiO_2 even with the omission of the calcination step will make the synthesis less energy intensive and will also reduce power consumption and costs. In addition, the hydrothermal method produces TiO_2 catalyst with high crystallinity and controlled particle size [30]. In a previous work, it was found that TiO_2 prepared via hydrothermal method gave an energy band gap lower than 3.0 eV even though it has anatase crystallite phase [30].

In this study, Fe–TiO_2 photocatalysts were synthesized by hydrothermal method without calcination. Box–Behnken Design (BBD) generated using Minitab 16.0 (Minitab, Inc., Pennsylvania, USA) was used to investigate the effects of hydrothermal temperature and time and Fe content (wt%) on the photocatalytic performance. Removal of reactive red 3 dye was done under UV light irradiation only, whereas alachlor photodegradation was performed under UV and visible light irradiation.

2. Materials and methods

2.1. Materials

Titanium tetrachloride ($TiCl_4$, 99%) from Merck Schuchardt OHG was used as the titanium dioxide catalyst precursor and 1,000 ppm Iron for atomic absorption standard as the dopant. Pure reactive red 3 (RR3, $C_{25}H_{15}ClN_7Na_3O_{10}S_3$) solid obtained from the textile industry was used to prepare a 1,000-ppm stock solution. Synthetic alachlor PESTANAL analytical standard (99.2%) was dissolved in HPLC grade distilled water from RCI Labscan Limited to prepare a 100-ppm stock solution. Hydrogen peroxide (H_2O_2, 30%) and ammonia solution (NH_4OH, 28%) were purchased from Ajax Finechem Pty Ltd and QRëc, respectively. Isocratic grade acetonitrile (CH_3CN, 99%) and methanol (CH_3OH, 99%) were purchased from Merck and RCI Labscan Limited, respectively.

2.2. Catalyst synthesis

The catalyst preparation followed previous works [18,30]. A solution of $TiCl_4$ dissolved in 400 mL cold deionized water was stirred for 30 min before the dropwise introduction of NH_4OH (90 mL). A white suspension resulted and this was stirred for another 30 min in an ice bath before it was centrifuged and decanted. Washing of the precipitates was done several times with deionized water until the pH of the washing becomes neutral. The precipitates were dried at 40˚C for 16 h and the obtained solid $Ti(OH)_4$ or amorphous TiO_2 was ground into fine powders manually.

Amorphous TiO_2 was dissolved in 30 mL H_2O_2 and this solution was stirred for 30 min in an ice bath. H_2O_2 (90 mL) was introduced dropwise into the solution. For the 0.10% and 0.20 wt% Fe-TiO_2 samples, 0.42 and 0.84 mL 1,000-ppm Fe^{3+} solution were added into the solution, respectively. The solution was continuously stirred for 4 h until it became transparent yellow. Thereafter, it was transferred to a Teflon-lined steel autoclave and was subjected to different hydrothermal temperature and time settings. The solution from the autoclave was filtered and dried as follows: (1) 40˚C for 2 h, (2) 100˚C for 4 h, and (3) 250˚C for 4 h.

2.3. Catalyst characterizations

X-ray diffraction analysis (XRD Model D8 Discover, Bruker AXS, Germany) was performed on Fe–TiO_2 catalysts to confirm the transformation of TiO_2 into the crystalline anatase phase. The following conditions were used: Cu Kα radiation at $\lambda = 0.15406$ nm, 40 kV potential, and 40 mA current. Scanning was done at a step of 1˚ $step^{-1}$ from 2θ of 20˚ to 70˚. Energy-dispersive X-ray spectroscopy (Oxford instrument, EDS7640, UK) was used on the pure TiO_2 photocatalyst. A UV–vis spectrophotometer (Specord 200 Plus, AnalytikJena, Germany) was used for the diffuse reflectance spectroscopy (UV-DRS) measurements, with $BaSO_4$ as the reflectance sample. X-ray absorption near edge structure (XANES) spectra were obtained for the Fe–TiO_2 samples using BL5.2: SUT-NANOTEC-SLRI XAS Beamline of Synchrotron Light Research Institute, Thailand. Brunauer–Emmett–Teller (BET) analysis (NOVA 1200e, Quantachrome, USA) was used to measure the specific surface areas of the photocatalysts.

Analysis of the remaining reactive red 3 dye concentrations was done using a UV–vis spectrophotometer (Specord 200 Plus, AnalytikJena) at 354 nm. On the other hand, analysis of the remaining alachlor concentrations was done using high-pressure liquid chromatography (Waters e2695 HPLC, Harlow Scientific, USA) at 197 nm, with a mixture of 40% methanol and 60% acetonitrile as the mobile phase at a flow rate of 1.0 mL min^{-1}. Injection volume was 20 μL. The separation was performed by a Hypersil C18 ODS 4.0 × 125 mm 5 μm column.

2.4. Catalyst activity measurements

The effects of hydrothermal temperature, hydrothermal time, and Fe content (wt%) during catalyst synthesis on RR3 removal was investigated using BBD (Table 1) created by using Minitab 16 (Minitab, Inc., Pennsylvania, USA). Initial RR3/alachlor concentration was set to 20 ppm, initial solution pH was adjusted to 4 using 1.0 M HNO_3, and catalyst loading was set to 1 g L^{-1} or 0.05 g per 50 mL. The suspensions were stirred at 500 rpm in the dark for the first 30 min to achieve equilibrium conditions. Afterwards, the suspensions were irradiated with UV light using three 20-W UVA lamps (Philips). The UVA light intensity was 0.335 mW cm^{-2}. Five-mL samples were collected after 15 and 30 min of reaction. Each sample was filtered using 0.45 μm nylon filter (Whatman) prior to chemical analysis. Addionally, photodegradation of alachlor was performed under visible light irradiation from three 22-W fluorescent lamps (Philips) for 60 min using the same amount catalyst and solution volume.

3. Results and discussion

The removal percentages of RR3 and alachlor after photocatalysis are shown in Table 2. In UV photocatalysis (30 min), the highest RR3 removal was 94% and the lowest was 76%. The highest and lowest alachlor removal under UV light irradiation (30 min) were 82 and 45%, respectively. On the other hand, under visible light irradiation (60 min), the highest and lowest alachlor removal were 51 and 15%, respectively. The alachlor removal percentages are lower than RR3

Table 1
Design of experiments for reactive red 3 dye/alachlor removal using Fe–TiO_2 catalysts

		Levels		
Factors	Symbol	−1	0	+1
Hydrothermal temperature (˚C)	X_1	150	175	200
Hydrothermal time (h)	X_2	8	16	24
Fe content (wt%)	X_2	0	0.10	0.20

Table 2
RR3 and alachlor removal under UV and visible light using Fe–TiO_2 photocatalysts

Run	Hydrothermal temperature (℃)	Hydrothermal time (h)	Fe content (wt%)	RR3 removal (%) UV		Alachlor removal (%)		
						UV		VIS
				15 min	30 min	15 min	30 min	60 min
1	150	8	0.1	89.40	93.44	22.15	48.49	28.24
2	175	16	0.1	70.62	85.95	29.75	49.70	19.00
3	175	16	0.1	76.42	89.88	21.55	47.21	20.39
4	200	8	0.1	82.39	90.44	24.58	44.94	28.97
5	175	16	0.1	83.46	91.30	21.99	48.22	24.98
6	150	24	0.1	73.38	90.02	22.66	46.90	16.85
7	150	16	0.2	89.12	94.10	21.65	46.44	20.25
8	175	8	0.0	71.37	89.19	48.92	75.74	33.98
9	175	8	0.2	91.92	93.37	22.84	45.07	21.28
10	200	16	0.2	77.66	83.81	21.62	48.56	14.91
11	200	16	0.0	66.16	93.51	46.71	82.43	51.02
12	150	16	0.0	85.29	88.33	44.38	70.62	19.79
13	175	24	0.2	75.45	81.11	33.59	48.33	17.64
14	200	24	0.1	70.30	76.31	26.47	52.68	22.86
15	175	24	0.0	79.07	85.70	30.39	55.17	19.40

removal percentages under UV light. This signifies that alachlor removal does not proceed as easily as color removal. Moreover, alachlor removal under visible light irradiation is significantly lower than RR3 and alachlor removal under UV light irradiation.

The estimated regression coefficients of full quadratic equations were calculated by least-square of error technique and displayed in Table 3 of RR3 and alachlor removal experiments. Then, the mathematical models for RR3 and alachlor removal are given in Eqs. (1)–(3):

$$Y_1 = 89.04 - 2.73X_1 - 4.16X_2 - 0.54X_3 - 2.68X_1X_2 - 3.87X_1X_3 - 2.19X_2X_3 + 0.55X_1^2 - 2.04X_2^2 + 0.34X_3^2 \quad (1)$$

$$Y_2 = 48.38 + 2.02X_1 - 1.40X_2 - 11.95X_3 + 2.33X_1X_2 - 2.42X_1X_3 + 5.96X_2X_3 + 2.91X_1^2 - 3.03X_2^2 + 10.73X_3^2 \quad (2)$$

$$Y_3 = 21.46 + 4.08X_1 - 4.47X_2 - 6.26X_3 + 1.32X_1X_2 - 9.14X_1X_3 + 2.74X_2X_3 + 3.10X_1^2 - 0.32X_2^2 + 1.94X_3^2 \quad (3)$$

where Y_1 is the percentage of RR3 removal under UV light irradiation (30 min); Y_2 and Y_3 are the percentages of alachlor removal under UV (30 min) and visible light (60 min) irradiation; X_1, X_2, and X_3 are the coded values of hydrothermal temperature, hydrothermal time, and Fe content, respectively; X_1X_2 is the interaction between hydrothermal temperature and hydrothermal time; X_1X_3 is the interaction between hydrothermal temperature and Fe content; X_2X_3 is the interaction between hydrothermal time and Fe content; and X_1^2, X_2^2, and X_3^2 are the quadratic terms for each of the main factors, respectively.

Table 4 shows the significant results of the ANOVA for the BBD on RR3 and alachlor removal. In RR3 removal under UV light, the response surface methodology (RSM) model generated is significant ($R^2 = 0.91$) and the lack-of-fit error is not significant. In Eq. (1), all of the main factors have negative coefficients indicating that increasing their levels would decrease RR3 removal (Table 3). The coefficients for the interactions also have negative values. The effects of hydrothermal time, X_2, and X_2^2, have the largest absolute value of coefficients and thus, the largest influence on the equation (Table 3). At 95% confidence, ANOVA results (Table 4) for RR3 removal under UV light (30 min) determined that the RSM model is also significant ($R^2 = 0.9299$) whereas the lack-of-fit error is not significant according to $F_{LOF} < F_{Critical}$ ($F_{critical(0.05,2,3)} = 9.55$). The main effects of hydrothermal temperature and hydrothermal time are significant on RR3 removal ($F_{Value} > F_{Critical}$ ($F_{critical(0.05,1,5)} = 6.61$), while Fe content is not signficant.

Alachlor removal under UV light (30 min) results, the main effect of Fe content on alachlor removal

Table 3
Estimated regression coefficients (β) for RR3 and alachlor removal using Fe–TiO_2 photocatalysts

Parameters	Coefficients	p-value	
(a) Estimated regression coefficients (β) for RR3 removal under UV light for 30 min			
Constant	89.04	0.000	Significant
A—hydrothermal temperature	−2.73	0.032	Significant
B—hydrothermal time	−4.16	0.006	Significant
C—Fe content	−0.54	0.583	Insignificant
A^2	0.55	0.702	Insignificant
B^2	−2.04	0.193	Insignificant
C^2	0.34	0.811	Insignificant
AB	−2.68	0.096	Insignificant
AC	−3.87	0.032	Significant
BC	−2.19	0.154	Insignificant
(b) Estimated regression coefficients (β) for alachlor removal under UV light for 30 min			
Constant	48.38	0.000	Significant
A—hydrothermal temperature	2.02	0.332	Insignificant
B—hydrothermal time	−1.40	0.492	Insignificant
C—Fe content	−11.95	0.001	Significant
A^2	2.91	0.342	Insignificant
B^2	−3.03	0.324	Insignificant
C^2	10.73	0.012	Significant
AB	2.33	0.421	Insignificant
AC	−2.42	0.405	Insignificant
BC	5.96	0.075	Insignificant
(c) Estimated regression coefficients (β) for alachlor removal under visible light for 60 min			
Constant	21.46	0.001	Significant
A—hydrothermal temperature	4.08	0.066	Insignificant
B—hydrothermal time	−4.47	0.051	Significant
C—Fe content	−6.26	0.016	Significant
A^2	3.10	0.282	Insignificant
B^2	−0.32	0.905	Insignificant
C^2	1.94	0.484	Insignificant
AB	1.32	0.615	Insignificant
AC	−9.14	0.014	Significant
BC	2.74	0.318	Insignificant

under UV light can be clearly seen in the relatively large negative coefficient of X_3 (−11.95), as well as in the large coefficient of its quadratic term, X_3^2 (10.73) as shown in Eq. (2). Fe content is significant in negative effect, while hydrothermal temperature and hydrothermal time are insignificant effects and the only hydrothermal temperature effect with a positive coefficient. The effect of hydrothermal temperature and the interaction effects have relatively small coefficients when compared to the coefficients assigned to the effect of Fe content. Although, the lack-of-fit error is significant ($F_{LOF} = 29.41$) according to $F_{LOF} > F_{Critical}$ ($F_{critical(0.05,2,3)} = 9.55$) at 95% confidence, the quadratic model generated is significant ($R^2 = 0.93$). Thus, the full quadratic equation can be used to predict the experimental results.

The quadratic equation for alachlor removal under visible light (60 min) is significant ($R^2 = 0.90$) and the ANOVA (Table 4) shows that the lack-of-fit error is not significant according to $F_{LOF} < F_{Critical}$ ($F_{critical(0.05,2,3)}$) at 95% confidence. In Eq. (3), the main effects of hydrothermal time and Fe content as well as the interaction between hydrothermal temperature and Fe content all have negative coefficients. Although hydrothermal temperature effect is insignificant at 95% confidence (p-value = 0.066), this effect is very close to the value of significant term (p-value = 0.05). Thus, we can conclude that all variables of main effects show significantly on alachlor removal under visible light at 60 min of reaction time. The interaction between hydrothermal temperature and Fe content has the highest coefficient and was already observed to have a significant effect.

Table 4
ANOVA for RR3 and alachlor removal using Fe–TiO_2 photocatalysts

Source	df	Sum of squares	Mean square	*F*-value	*p*-value	
(a) RR3 removal under UV light for 30 min						
Regression	9	326.244	36.249	5.31	0.040	Significant
A—hydrothermal temperature	1	59.514	59.514	8.72	0.032	Significant
B—hydrothermal time	1	138.611	138.611	20.30	0.006	Significant
C—Fe content	1	2.354	2.354	0.34	0.583	Insignificant
A^2	1	1.125	1.125	0.16	0.702	Insignificant
B^2	1	15.410	15.410	2.26	0.193	Insignificant
C^2	1	0.432	0.432	0.06	0.811	Insignificant
AB	1	28.676	28.676	4.20	0.096	Insignificant
AC	1	59.830	59.830	8.76	0.032	Significant
BC	1	19.228	19.228	2.82	0.154	Insignificant
Lack-of-fit	3	18.774	6.258	0.81	0.592	Insignificant
(b) Alachlor removal under UV light for 30 min						
Regression	9	1,878.20	208.69	7.36	0.020	Significant
A—hydrothermal temperature	1	32.64	32.64	1.15	0.322	Insignificant
B—hydrothermal time	1	15.57	15.57	0.55	0.492	Insignificant
C—Fe content	1	1,141.54	1,141.54	40.28	0.001	Significant
A^2	1	31.17	31.17	1.10	0.342	Insignificant
B^2	1	33.89	33.89	1.20	0.324	Insignificant
C^2	1	425.22	425.22	15.01	0.012	Significant
AB	1	21.76	21.76	0.77	0.421	Insignificant
AC	1	23.47	23.47	0.83	0.405	Insignificant
BC	1	141.97	141.97	5.01	0.075	Insignificant
Lack-of-fit	3	138.55	46.18	29.41	0.033	Significant
(c) Alachlor removal under visible light for 60 min						
Regression	9	1,025.56	1,025.56	4.68	0.052	Significant
A—hydrothermal temperature	1	133.09	133.09	5.47	0.066	Insignificant
B—hydrothermal time	1	159.49	159.49	6.56	0.051	Significant
C—Fe content	1	313.88	313.877	12.90	0.016	Significant
A^2	1	35.58	35.58	1.45	0.282	Insignificant
B^2	1	0.383	0.383	0.02	0.905	Insignificant
C^2	1	425.22	425.22	15.01	0.012	Significant
AB	1	6.97	6.97	0.29	0.615	Insignificant
AC	1	334.34	334.34	13.17	0.014	Significant
BC		29.92	29.92	1.23	0.318	Insignificant
Lack-of-fit	3	102.03	34.011	3.47	0.232	Not significant

Both of the other interactions are positive but have smaller coefficients and were not found to be significant in alachlor removal under visible light.

Furthermore, optimization of the parameters were determined using BBD. The optimum conditions for RR3 removal under UV light irradiation were 150˚C, 8 h, and 0.20 wt% Fe. Based on Eq. (1), low hydrothermal temperature and hydrothermal time settings are already known to be favored in this model and Fe content has a very small negative effect. On the other hand, the optimum conditions for alachlor removal are the same for UV and visible light irradiation, which are 200˚C, 8 h, and 0 wt% Fe.

The effects of the main factors on RR3 and alachlor removal are shown in Fig. 1. In RR3 removal under UV light (Fig. 1(a)), all of the main factors have negative effects. The effects of hydrothermal temperature and hydrothermal time are significant and increasing these hydrothermal settings decreases RR3 removal under UV light. The effect of Fe content is not significant since the mean RR3 removal percentages were at a very small range for the three different amounts of Fe added.

The mean alachlor removal under UV light irradiation is lower than the mean RR3 removal. The mean alachlor removal under visible light irradiation is

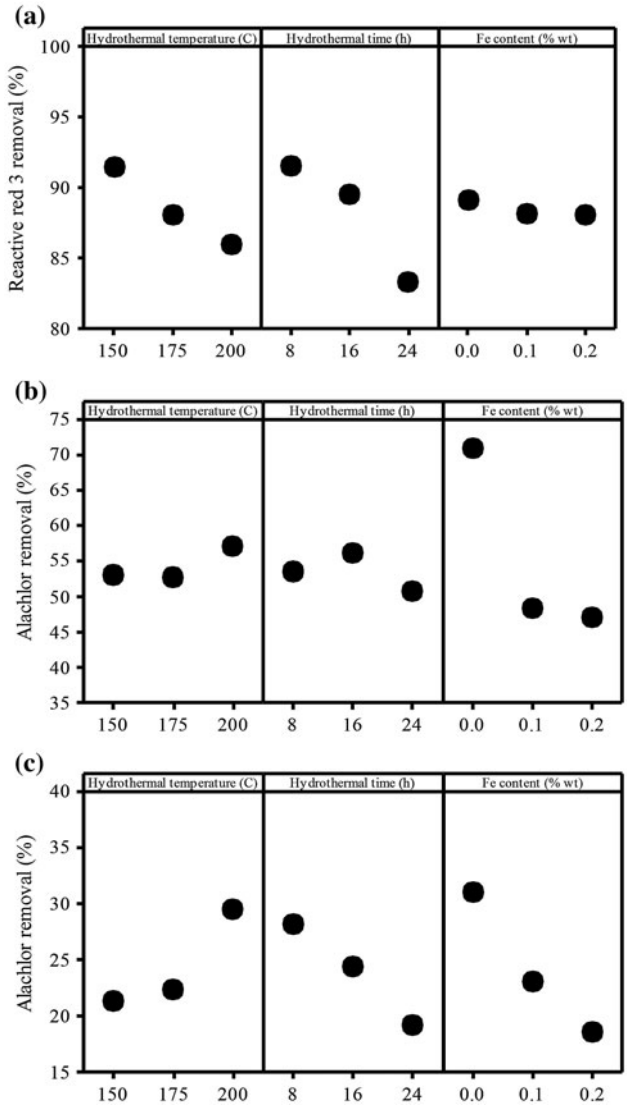

Fig. 1. Main effects for (a) RR3 removal under UV light and alachlor removal under, (b) UV light, and (c) visible light irradiation (initial RR3/Alachlor concentration: 20 ppm, pH 4.0 and catalyst loading 1 g L^{-1}).

much lower than that under UV light irradiation. The main effects plots for alachlor removal under UV and visible light (Fig. 1(b) and (c)) show trends that are similar to each other but contrary to RR3 removal (Fig. 1(a)). The only significant effect in alachlor removal is the Fe content, in which the samples without Fe-doping gave the highest mean alachlor removal under UV and visible light irradiation, as also exhibited in Eqs. (2) and (3). Varying the hydrothermal temperature and time did not notably increase or decrease alachlor removal whether under UV light or visible light irradiation.

In RR3 removal, only the interaction between the hydrothermal temperature and Fe content is significant. High RR3 removal was observed when the hydrothermal temperature was decreased and the Fe content is increased. Apart from this, the mean removal percentages almost do not vary greatly within the range of values in each interaction effect investigated. Fig. 2(a)–(c) show the contour plots for this interaction. The results of these two plots show that the highest RR3 removal can be observed when the Fe content is 0.20 wt% and the hydrothermal temperature used was 150˚C. This affirms the importance of Fe doping that although the main effect of Fe content is insignificant, doping with 0.20 wt% does not reduce the removal efficiency.

From ANOVA (Table 4), none of the interaction effects are significant in alachlor removal under UV light irradiation (at 95% confidence). Following the obtained optimum conditions, fixing the Fe content to 0 wt%, the highest alachlor removal is observed when the hydrothermal temperature is 200˚C and when the hydrothermal time is 8 h.

Similar to RR3 removal in UV and visible light, the interaction between hydrothermal temperature and Fe content is significant in alachlor removal under visible light. From Fig. 2(b) and (c), the highest alachlor removal was achieved when the hydrothermal temperature is at 200˚C and the Fe content is at 0 wt% which is the exact opposite of the preferred interaction in RR3 removal.

These findings are supported by the results of the characterization techniques. The XRD patterns of Fe–TiO_2 photocatalysts are shown in Fig. 3, comparing the effects of hydrothermal temperature, hydrothermal time, and Fe content. The characteristic peaks of anatase TiO_2 at the 2θ positions of 25˚, 38˚, 48˚, 55˚, 56˚, and 63˚ are found in all samples. This confirms that anatase TiO_2 has been produced via the hydrothermal treatment without calcination. Anatase TiO_2 is the component of the catalyst that is responsible for its photocatalytic activity. No Fe-containing peaks have been detected since the doping was done in small amounts [16]. Fe-doping also has no effect on the degree of crystallinity since there is no change in the sharpness of the main peaks of anatase for the samples with 0% and 0.20 wt% Fe.

The crystallite sizes of the photocatalysts were calculated using Scherrer's equation based on the XRD patterns. For catalysts synthesized at hydrothermal time of 8 h and 0 wt% Fe, an increase in the hydrothermal temperature from 150 to 200˚C resulted in an increase (21%) in crystallite size from 10.53 nm

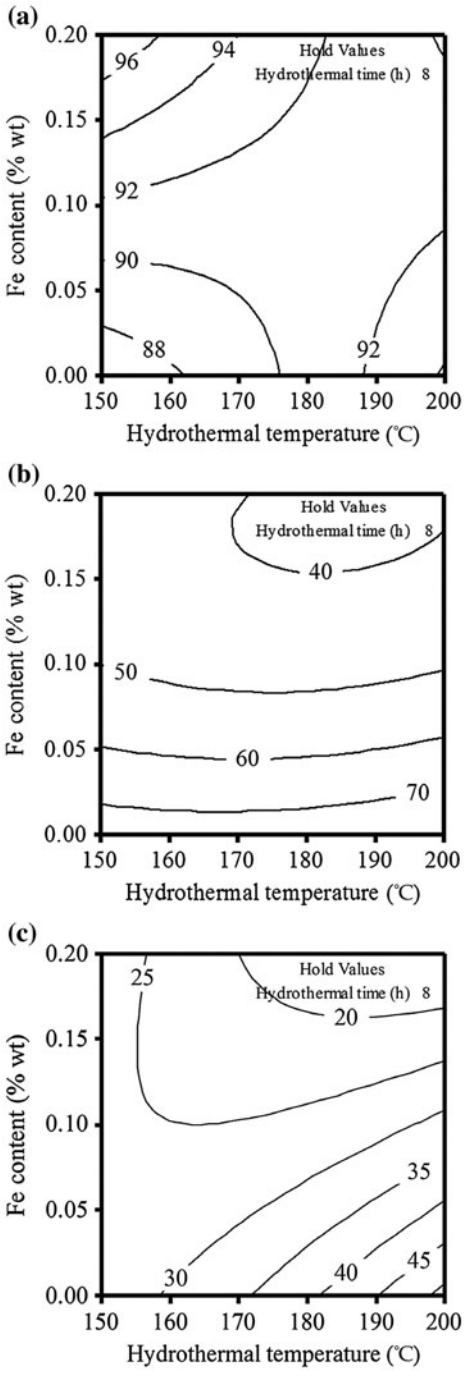

Fig. 2. Contour plots for the interaction hydrothermal temperature and Fe content on RR3 dye and alachlor removal at 8 h of hydrothermal time (initial RR3/Alachlor concentration: 20 ppm, pH 4.0 and catalyst loading 1 g L^{-1}).

to 12.74 nm, which then translates to an increase in particle size. The increase in crystallite size brought about by the increase in hydrothermal temperature enhanced RR3 and alachlor removal. At hydrothermal

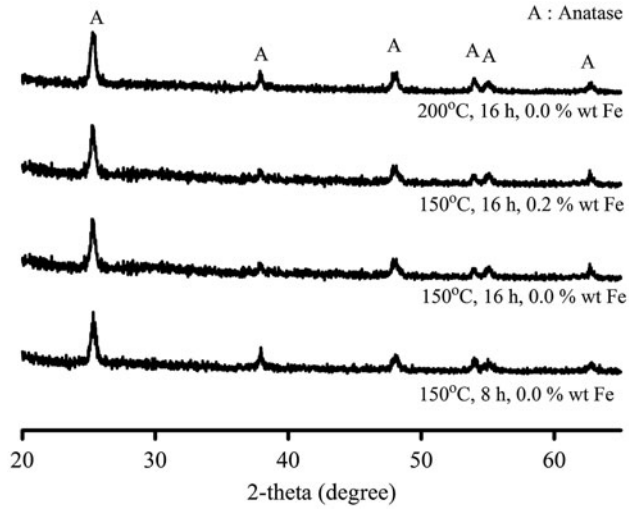

Fig. 3. XRD patterns of Fe–TiO_2 photocatalysts. This samples show only anatase crystallite phase.

time of 8 h and 0 wt% Fe, increasing the hydrothermal temperature from 150 to 200˚C increased RR3 removal (UV light) from 88 to 94%; alachlor removal (UV light) from 71 to 82%; and alachlor (visible light) from 20 to 51%.

The crystallite size of TiO_2 is directly related to its particle size. BET surface area is known to be indirectly proportional to crystallite size [31]. For samples with 0.1 wt% Fe at hydrothermal time of 8 h, increasing the hydrothermal temperature from 150 to 200˚C increased the BET surface area from 67.26 to 74.62 $m^2 g^{-1}$. Thus, this also translates to a decrease in crystallite size. In UV photocatalysis, increasing the hydrothermal temperature from 150 to 200˚C decreased RR3 removal from 93 to 90% and alachlor removal from 48 to 45%. Alachlor removal under visible light irradiation did not significantly change from 28 to 29%.

Increasing the hydrothermal time from 8 to 16 h resulted in a decrease (15%) in crystallite size from 12.15 to 10.53 nm for catalysts synthesized at a hydrothermal temperature of 150˚C and with 0 wt% Fe. On the other hand, at the hydrothermal temperature of 150˚C and Fe content of 0.1 wt% Fe, increasing the hydrothermal time from 8 to 24 h increased the BET surface area from 67.26 to 87.87 $m^2 g^{-1}$, which also corresponds to a decrease in crystallite size. In UV photocatalysis, RR3 removal decreased from 93 to 90% while alachlor removal decreased from 48 to 47%. Alachlor removal under visible light irradiation also decreased from 28 to 17%.

A decrease in crystallite size that corresponds to the increase in BET surface area brought about by

increasing the hydrothermal temperature from 150 to 200˚C and the hydrothermal time from 8 to 24 h is observed in samples containing 0.1 wt% Fe. The atomic size of Fe (r = 0.64 Å) is very similar to that of Ti (r = 0.68 Å) [32]. Thus, its insertion into the crystal lattice of TiO_2 did not cause any major alterations in the structure that will decrease the crystallinity. The slightly smaller atomic size of Fe may have caused a slight decrease in the effective crystallite size of the Fe–TiO_2 photocatalysts. The insertion of Fe^{3+} into the Ti^{4+} structure translates into defects which affected the crystallite growth [32].

In order to confirm the state of Fe-doping, XANES was used to determine the valence states in the photocatalysts as shown in Table 5. For different Fe–TiO_2 photocatalysts containing 0.20 wt% Fe, the different hydrothermal temperature and time settings resulted in a mixture of Fe^{3+} and $Fe^{3+/4+}$ species. An increase in hydrothermal time from 8 to 16 h resulted in a major shift of the valence state from Fe^{3+} to a combination of $Fe^{3+/4+}$. Fe^{4+} is stable in the lattice of anatase TiO_2, which indicates that it can substitute the Ti atom easily. On the other hand, increasing the hydrothermal temperature from 150 to 175˚C only resulted in a slight decrease in the amount of Fe^{3+} species. In general, the majority of the measurements also denoted that there are no species in the Fe^{2+} state. The XANES results showing that the majority of the Fe species has a +3 valence state is further supported by the energy band gap measurements from the UV-DRS characterization. Kubelka-Munk theory was used to obtain the absorption spectra and energy band gap measurements. Pure TiO_2 photocatalysts obtained in this study registered an energy band gap of 2.78 eV. Fe–TiO_2 doped with 0.10 wt% Fe also exhibited an energy band gap of 2.72 eV. This means that the doping amount was too small to significantly cause a change in the absorption properties of pure TiO_2 synthesized by the same method. However, the addition of 0.20 wt% Fe decreased this value to 2.60 eV. This shift can only be attributed to the presence of Fe^{3+}, which was confirmed by the XANES measurements. Additionally, the measured energy band gaps for the synthesized Fe–TiO_2 photocatalysts with 0.00, 0.10, and 0.20 wt% Fe in this study are about 2.78, 2.72, and 2.60, respectively, and significantly lower than the reported value of 3.20 eV for TiO_2 in most studies. Although the decrease in energy band gap is expected for the Fe-doped TiO_2 as ascribed to the red shift phenomenon [16,30], the measured energy band gap for the undoped TiO_2 is still low enough to ensure its activity even in visible light photocatalysis. From a previous work [30], pure TiO_2 prepared by same technique has shown the energy band gap lower than 3.00 eV. The energy-dispersive X-ray results of the pure TiO_2 photocatalyst have Ti, O, and N as the main elements at about 51.19, 38.78, and 10.03 wt%, respectively. According to another research [33], the preparation of amorphous TiO_2 in alkaline conditions by precipitation using NH_3OH resulted with N as an impurity in the amorphous TiO_2. It is also well known that N is one of the non-metal dopants that decrease the energy band of TiO_2 [34,35]. Thus, it can be concluded that nitrogen doping is one of the major causes of the red shift of the energy band gap.

From the characterization techniques, it was confirmed that the Fe^{3+} and N present in the photocatalysts decreased the energy band gap and thus, increased the absorption in visible light. However, alachlor removal under both UV and visible light irradiation favored TiO_2 than Fe-doped TiO_2. In this case, the decreased activity may be due to the behavior of Fe^{3+} as traps for the photogenerated electron–hole pairs. Instead of discretely trapping the electrons and the holes, the traps themselves may have become the recombination centers [18]. This was not observed in the experiments in RR3 color removal under UV light irradiation, wherein the optimum condition for Fe content is 0.20 wt% Fe. Dye sensitization also occurs under UV light irradiation in which the dye molecules of RR3 are able to supply excess electrons to the system that enhances the photocatalytic activity [18]. Another reason for the higher activity of Fe–TiO_2 with 0.20 wt% Fe in RR3 removal under UV light irradiation is the basis of RR3 removal percentages is only the decolorization as measured by spectrophotometry.

Table 5
XANES measurements of the valence states of Fe in Fe–TiO_2 photocatalysts

Catalyst		Valence state	
Hydrothermal temperature (˚C)	Hydrothermal time (h)	Fe^{3+}	$Fe^{3+/4+}$
150	8	75.3	24.7
150	16	8.6	91.4
175	8	66.8	33.2

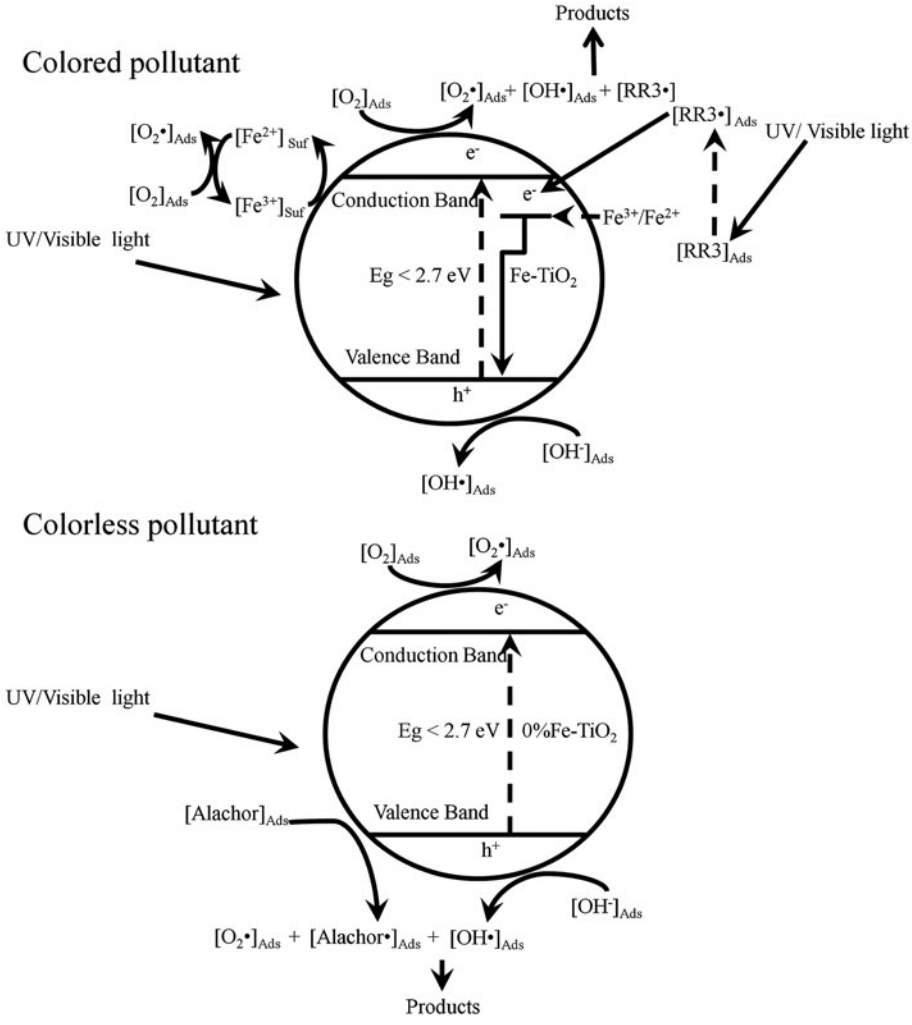

Fig. 4. Mechanisms of RR3 and alachlor degradation over Fe–TiO_2 photocatalysts under UV–vis light irradiation.

RR3 is also an organic molecule like alachlor. Alachlor degradation was reported in terms of the remaining amounts in solution as measured by the HPLC. The breakdown of the organic molecule of RR3 was not taken into account and thus decolorization gave higher removal rates than the alachlor removal. Therefore, the enhancement of TiO_2 by Fe doping was only observed in reactive red 3 dye removal under UV photocatalysis. Such effect was not significantly detected in the alachlor removal experiments under both UV and visible light irradiation. Even so, the undoped TiO_2 photocatalysts are already active under visible light irradiation and can remove up to 51.02% alachlor from the solution after 60 min. Regardless of the Fe-doping, the energy band gap of the pure TiO_2 is already lower than the reported value in literature of 3.20 eV, which explains its activity in both UV and visible light regions.

The mechanisms for the photodegradation of RR3 and alachlor under UV light irradiation can be explained in different mechanisms, depending on the amount of Fe doped on TiO_2. The electrons in the TiO_2 valence band can be excited by light energy and move to conduction band. The mechanisms of RR3 photodegradation include four pathways, as shown in Fig. 4. Path 1 shows electrons form RR3* radicals, excited by light irradiation to RR3, which moved to Fe^{3+}. Similar to a photosensitization process, the electrons moved to the valence band of TiO_2 to react with the holes to decrease the electron–hole pair recombination of TiO_2 according to castro and coworkers providing this mechanism in their work [19]. Path 2 shows OH^- on the surface of TiO_2 reacting with the holes and forming hydroxyl radicals (·OH). The ·OH radical then reacted with adsorbed RR3 to degrade it to smaller molecules as explained in the authors's previous

works [16]. Path 3 shows electrons in the conduction band reacting with the surface-adsorbed O_2 molecules to yield $O_2^{-\cdot}$ radicals. Consequently, the $O_2^{-\cdot}$ radicals reacted with adsorbed RR3 to break its molecules. Path 4 shows the Fe^{3+} on the surface of TiO_2 being excited (photosensitization) and bringing about efficient charge transfer in the composite samples. The Fe^{3+} particles could also act as electron traps as explained in the our previous work [16]. These could reduce electron recombination in the catalyst matrix by becoming Fe^{2+} species. Since Fe^{2+} is unstable, it would rapidly transfer an electron into the O_2 molecules to yield more $O_2^{-\cdot}$ radicals. Therefore, the photocatalytic activity of TiO_2 doped with Fe could be improved greatly for RR3 dye, which is a colored pollutant in agreement with many researches [9,15,19,36]. On the other hand, the mechanisms of alachlor photodegradation included only two pathways that are the same with that of RR3 in paths 2 and 3, as shown in Fig. 4. The colorless pollutant photodegradation under UV light irradiation cannot be enhanced efficiently by Fe-doping in TiO_2 as was also reported by other researchers [19,37].

4. Conclusions

Fe–TiO_2 catalysts were synthesized via hydrothermal method without calcination. Photocatalytic degradation of reactive red 3 dye was carried out under UV light irradiation whereas alachlor photodegradation was carried out under UV and visible light irradiation. Under UV light irradiation, the highest removal percentages for reactive red 3 dye were 92 and 94% for 15 and 30 min, respectively. In UV photocatalysis of RR3 dye for 30 min, the significant main effects are the hydrothermal temperature and time and the interaction between hydrothermal temperature and Fe content. The obtained optimum conditions are 150˚C, 8 h, and 0.20 wt% Fe. Photodegradation of alachlor under UV light irradiation for 15 and 30 min gave removal percentages of 49 and 82%, respectively. Visible light photocatalysis for 60 min removed up to 51% of alachlor in the solution. Only Fe content is the significant main effect in both experiments, wherein alachlor removal is highest when Fe content is 0. Under UV and visible light photocatalysis, the optimum conditions are 200˚C, 8 h, and 0.00 wt% Fe.

Acknowledgments

The authors would like to thank Research Center for Environmental and Hazardous Substance Management (EHSM), Khon Kaen University and the Department of Science and Technology, Philippines through the Engineering Research and Development for Technology (ERDT) for the financial support given to this research. The authors also acknowledge the Synchrotron Light Research Institute (public organization) Thailand for the courtesy on the XANES measurement (BL5.2: SUT-NANOTEC-SLRI XAS Beamline).

References

[1] K. Hashimoto, H. Irie, A. Fujishima, TiO_2 photocatalysis: A historical overview and future prospects, Jpn. J. Appl. Phys. 44(12) (2005) 8269–8285.
[2] Y. Wu, J. Zhang, L. Xiao, F. Chen, Properties of carbon and iron modified TiO_2 photocatalyst synthesized at low temperature and photodegradation of acid orange 7 under visible light, Appl. Surf. Sci. 256 (2010) 4260–4268.
[3] S. Artkla, K. Wantala, B. Srinameb, N. Grisdanurak, W. Klysubun, J. Wittayakun, Characteristics and photocatalytic degradation of methyl orange on Ti-RH-MCM-41 and TiO_2/RH-MCM-41, Korean J. Chem. Eng. 26 (2009) 1556–1562.
[4] S. Liu, Y. Chen, Enhanced photocatalytic activity of TiO_2 powders doped by Fe unevenly, Catal. Commun. 10 (2009) 894–899.
[5] E. Piera, Relationship concerning the nature and concentration of Fe(III) species on the surface of TiO_2 particles and photocatalytic activity of the catalyst, Appl. Catal. B: Environ. 46 (2003) 671–685.
[6] Z. Ambrus, N. Balázs, T. Alapi, G. Wittmann, P. Sipos, A. Dombi, et al., Synthesis, structure and photocatalytic properties of Fe(III)-doped TiO_2 prepared from $TiCl_3$, Appl. Catal. B: Environ. 81 (2008) 27–37.
[7] C.A. Castro-López, A. Centeno, S.A. Giraldo, Fe-modified TiO_2 photocatalysts for the oxidative degradation of recalcitrant water contaminants, Catal. Today 157 (2010) 119–124.
[8] Y. Wu, J. Zhang, L. Xiao, F. Chen, Preparation and characterization of TiO_2 photocatalysts by Fe^{3+} doping together with Au deposition for the degradation of organic pollutants, Appl. Catal. B: Environ. 88 (2009) 525–532.
[9] J. Zhu, J. Ren, Y. Huo, Z. Bian, H. Li, Nanocrystalline Fe/TiO_2 visible photocatalyst with a mesoporous structure prepared via a nonhydrolytic sol–gel route, J. Phys. Chem. C 111 (2007) 18965–18969.
[10] T.K. Ghorai, S.K. Biswas, P. Pramanik, Photooxidation of different organic dyes (RB, MO, TB, and BG) using Fe(III)-doped TiO_2 nanophotocatalyst prepared by novel chemical method, Appl. Surf. Sci. 254 (2008) 7498–7504.
[11] T. Tong, J. Zhang, B. Tian, F. Chen, D. He, Preparation of Fe^{3+}-doped TiO_2 catalysts by controlled hydrolysis of titanium alkoxide and study on their photocatalytic activity for methyl orange degradation, J. Hazard. Mater. 155 (2008) 572–579.
[12] J.H. Jho, D.H. Kim, S.J. Kim, K.S. Lee, Synthesis and photocatalytic property of a mixture of anatase and rutile TiO_2 doped with Fe by mechanical alloying process, J. Alloys Compd. 459 (2008) 386–389.

[13] M.A. Khan, S.I. Woo, O.B. Yang, Hydrothermally stabilized Fe(III) doped titania active under visible light for water splitting reaction, Int. J. Hydrogen Energy 33 (2008) 5345–5351.
[14] M.S. Nahar, K. Hasegawa, S. Kagaya, Photocatalytic degradation of phenol by visible light-responsive iron-doped TiO_2 and spontaneous sedimentation of the TiO_2 particles, Chemosphere 65 (2006) 1976–1982.
[15] K. Wantala, L. Laokiat, P. Khemthong, N. Grisdanurak, K. Fukaya, Calcination temperature effect on solvothermal Fe–TiO_2 and its performance under visible light irradiation, J. Taiwan Inst. Chem. Eng. 41 (2010) 612–616.
[16] K. Wantala, P. Khemthong, J. Wittayakun, N. Grisdanurak, Visible light-irradiated degradation of alachlor on Fe–TiO_2 with assistance of H_2O_2, Korean J. Chem. Eng. 28 (2011) 2178–2183.
[17] K. Wantala, D. Tipayarom, L. Laokiat, N. Grisdanurak, Sonophotocatalytic activity of methyl orange over Fe(III)/TiO_2, React. Kinet. Catal. Lett. 97 (2009) 249–254.
[18] M.D.G. de Luna, K.K.P. Rivera, T. Suwannaruang, K. Wantala, Alachlor photocatalytic degradation over uncalcined Fe–TiO_2 loaded on granular activated carbon under UV and visible light irradiation, Desalin Water Treat. (2015), doi: 10.1080/19443994.2015.1011706.
[19] C.A. Castro, A. Centeno, S.A. Giraldo, Iron promotion of the TiO_2 photosensitization process towards the photocatalytic oxidation of azo dyes under solar-simulated light irradiation, Mater. Chem. Phys. 129 (2011) 1176–1183.
[20] M. Kang, Synthesis of Fe/TiO_2 photocatalyst with nanometer size by solvothermal method and the effect of H_2O addition on structural stability and photodecomposition of methanol, J. Mol. Catal. A: Chem. 197 (2003) 173–183.
[21] R.J. Tayade, R.G. Kulkarni, R.V. Jasra, Transition metal ion impregnated mesoporous TiO_2 for photocatalytic degradation of organic contaminants in water, Ind. Eng. Chem. Res. 45 (2006) 5231–5238.
[22] L. Wen, B. Liu, X. Zhao, K. Nakata, T. Murakami, A. Fujishima, Synthesis, characterization, and photocatalysis of Fe-doped TiO_2: A combined experimental and theoretical study, Int J Photoenergy 2012 (2012) 1–10, doi: 10.1155/2012/368750.
[23] W.C. Oh, F.J. Zhang, Z. Meng, K. Zhang, Relative photonic properties of Fe/TiO_2-nanocarbon catalysts for degradation of MB solution under visible light, Bull. Korean Chem. Soc. 31 (2010) 1128–1134.
[24] M.I. Litter, J.A. Navío, Photocatalytic properties of iron-doped titania semiconductors, J. Photochem. Photobiol., A 98 (1996) 171–181.
[25] M. Asiltürk, F. Sayılkan, E. Arpaç, Effect of Fe^{3+} ion doping to TiO_2 on the photocatalytic degradation of Malachite Green dye under UV and vis-irradiation, J. Photochem. Photobiol., A 203 (2009) 64–71.
[26] K. Wantala, P. Sriprom, N. Pojananukij, A. Neramittagapong, S. Neramittagapong, P. Kasemsiri, Optimal decolorization efficiency of Reactive Red 3 by Fe-RH-MCM-41 catalytic wet oxidation coupled with Box–Behnken design, Key Eng. Mater. 545 (2013) 109–114.
[27] E.S. Bireller, P. Aytar, S. Gedikli, A. Cabuk, Removal of some reactive dyes by untreated and pretreated saccharomyces cerevisiae, an alcohol fermentation waste, J. Sci. Ind. Res. India 71 (2012) 632–639.
[28] S. Galassi, A. Provini, S. Mangiapan, E. Benfenati, Alachlor and its metabolites in surface water, Chemosphere 32 (1996) 229–237.
[29] C.W. Knapp, D.W. Graham, G. Berardesco, F. deNoyelles, B.J. Cutak, C.K. Larive, Nutrient level, microbial activity, and alachlor transformation in aerobic aquatic systems, Water Res. 37 (2003) 4761–4769.
[30] T. Suwannaruang, K.K.P. Rivera, A. Neramittagapong, K. Wantala, Effects of hydrothermal temperature and time on uncalcined TiO_2 synthesis for Reactive Red 120 photocatalytic degradation, Surf. Coat. Technol. 271 (2015) 192–200.
[31] N.A. Jamalluddin, A.Z. Abdullah, Reactive dye degradation by combined Fe(III)/TiO_2 catalyst and ultrasonic irradiation: Effect of Fe(III) loading and calcination temperature, Ultrason. Sonochem. 18 (2011) 669–678.
[32] C.J.E. Bajamundi, M.L.P. Dalida, K. Wantala, P. Khemthong, N. Grisdanurak, Effect of Fe^{3+} doping on the performance of TiO_2 mechanocoated alumina bead photocatalysts, Korean J. Chem. Eng. 28 (2011) 1688–1692.
[33] Y.F. Li, W.P. Zhang, X. Li, Y. Yu, TiO_2 nanoparticles with high ability for selective adsorption and photodegradation of textile dyes under visible light by feasible preparation, J. Phys. Chem. Solids 75 (2014) 86–93.
[34] S.S. Shinde, C.H. Bhosale, K.Y. Rajpure, Photodegradation of organic pollutants using N-titanium oxide catalyst, J. Photochem. Photobiol. B 141 (2015) 186–191.
[35] Y.-G. Kang, K.-H. Lee, H.-S. Hahm, Preparation of visible light sensitive nano-sized N-TiO_2 photocatalysts and their photocatalytic activity under visible light, Turk. J. Chem. 39 (2015) 159–168.
[36] N.J. Peill, L. Bourne, M.R. Hoffmann, Iron(III)-doped Q-sized TiO_2 coatings in a fiber-optic cable photochemical reactor, J. Photochem. Photobiol., A 108 (1997) 221–228.
[37] N. Wetchakun, K. Chiang, R. Amal, S. Phanichphant, Synthesis and characterization of transition metal ion doping on the photocatalytic activity of TiO_2 nanoparticles, in: 2nd IEEE Int Nanoelectron Conf, 2008, pp. 43–47. Available from: <http://www.scopus.com/record/display.uri?eid=2-s2.0-52649172814&origin=resultslist&sort=plf-f&src=s&st1=Synthesis+and+characterization+of+transition+metal+ion+doping+on+the+photocatalytic+activity+of+TiO2+nanoparticles&st2=&sid=07A1B083CBE469E305655A4B67A8FCF1.aqHV0EoE4xlIF3hgVWgA%3a200&sot=b&sdt=b&sl=129&s=TITLE-ABS-KEY%28Synthesis+and+characterization+of+-transition+metal+ion+doping+on+the+photocatalytic+activity+of+TiO2+nanoparticles%29&relpos=0&citeCnt=1&searchTerm=TITLE-ABS-KEY%28Synthesis+and+characterization+of+transition+metal+ion+doping+on+the+photocatalytic+activity+of+TiO2+nanoparticles%29>.